Correspondence to:

X. Jiang,
xjiang7@uh.edu

Impact of El Niño Southern Oscillation on CO2 and Solar-Induced Fluorescence Over the Indo-Pacific Region

Ronald Albright[1] , Thishan D. K. Gamalathge[1], Xinyue Wang[1], Xun Jiang[1] , and Liming Li[2]

[1]Department of Earth & Atmospheric Sciences, University of Houston, Houston, TX, USA, [2]Department of Physics, University of Houston, Houston, TX, USA

Abstract Over the tropical Indo-Pacific, we explore the variations of Solar-Induced Fluorescence (SIF), CO_2, and precipitation during El Niño Southern Oscillation (ENSO) events verse other times. Based on various data sets, we analyze the time series of deseasonalized precipitation, vertical velocity, SIF, and CO_2 across the Indo-Pacific region. Our analysis reveals that there is less precipitation, more sinking air, lower SIF, and higher carbon dioxide over the Indo-Pacific region during the El Niño events compared to other times. We also explore the spatial patterns of different variables to gain a deeper understanding of their relationships. The spatial analysis suggests that less precipitation resulting from predominant sinking air not only leads to lower SIF values by reducing photosynthetic activities but also triggers more biomass burning, which contribute to an increase in atmospheric CO_2 levels across most areas of the Indo-Pacific region. The comparative study between observational analyses and numerical simulation by the NOAA CarbonTracker model indicates that the model can simulate the increase of atmospheric column CO_2 during the El Niño event, although there are some difficulties in capturing the correct spatial pattern. The results of this study can significantly enhance our understanding of the spatial-temporal variabilities of atmospheric CO_2 concentration and the observational characteristics can be used to enhance models. Furthermore, the complex interactions between ENSO and other variables revealed in this study improve our understanding of how ENSO influences the biosphere and carbon cycle.

1. Introduction

While climate change's devastating impacts are increasing, people and researchers are becoming more interested in the science behind it. The global annual increase of atmospheric CO_2 is nearly 2 ppm per year (Keeling et al., 1995; Lan et al., 2023), which has a significant impact on global warming (IPCC, 2013). Beyond the long-term trend, atmospheric concentrations of CO_2 are also subject to influence from large-scale circulations (e.g., Jiang & Yung, 2019; Jiang et al., 2010; Li et al., 2010; Liu et al., 2017).

The El Niño-Southern Oscillation (ENSO) is characterized by recurring changes in sea surface temperatures and trade winds (Bjerknes, 1966, 1969). It is found that ENSO can modulate CO_2 concentration at the surface (Bacastow, 1976). The cessation of the rising ocean water reduces the amount of carbon-rich water brought to the ocean surface, leading to a decrease in the amount of CO_2 released from the ocean into the atmosphere (e.g., Feely, 1987; Feely et al., 2006). Additionally, an increase in respiration during ENSO events causes the terrestrial biosphere to become a more significant source of atmospheric CO_2 (e.g., Francey et al., 1995; Jones et al., 2001). The net result is an increase in the CO_2 growth rate during ENSO events from both ocean and land sources (e.g., Jones et al., 2001).

This paper aims to examine the impact of ENSO on atmospheric CO_2 concentration and biosphere photosynthesis in the Indo-Pacific region. The Indo-Pacific region is chosen due to its inclusion of the New Guinea Rainforest, the third-largest tropical rainforest, spanning approximately 71 million acres across Indonesia and Papua New Guinea. This rainforest serves as a significant sink of atmospheric CO_2. To track biosphere photosynthetic activities, we utilize Solar-Induced Fluorescence (SIF). Additionally, we analyze satellite column CO_2 data, precipitation, transport, and burned area to investigate the interaction between the biosphere and the atmosphere during the El Niño months. The CarbonTracker model is also employed to assess the impact of ENSO on CO_2, aiding in our understanding of whether the model accurately simulates CO_2 variations in the Indo-Pacific region.

2. Data and Models

The methodology employed in this investigation involves the analysis of space-based and ground-based measurements, including (a) SIF retrievals from satellite Orbiting Carbon Observatory 2 (OCO-2), (b) CO_2 Column retrievals from OCO-2, (c) Southern Oscillation Index (SOI), (d) Multivariate ENSO Index version 2 (MEIv2), (e) NCEP2 meteorological data, (f) Burned area data from MODIS, (g) Global precipitation data from GPCP version 2.3, and (h) GFEDv4.1 CO_2 surface emissions data.

2.1. OCO-2 SIF and OCO-2 Column CO_2 Data

To examine CO_2 and photosynthetic activity in the Indo-Pacific region during the El Niño months, we use column CO_2 retrieved from three high-resolution spectral reflectance (sunlight) bands (A-Band 0.76 μm, near-infrared 1.61 and 2.06 μm) and SIF retrievals from OCO-2 (Crisp et al., 2017; Frankenberg et al., 2014). Both OCO-2 column CO_2 and SIF retrievals exhibit good agreement with surface and airborne measurements (Wunch et al., 2017; Yu et al., 2018). The OCO-2 SIF and Column CO_2 data retrievals have been regridded to a 2° × 2° resolution (latitude and longitude).

2.2. Southern Oscillation Index (SOI)

SOI is a metric calculated by taking the sea level pressure differences between Darwin and Tahiti (Trenberth, 1984). It is used to examine the spatial distributions of SIF, CO_2, and precipitation during El Niño events versus other months. A negative (positive) SOI value indicates an El Niño (La Niña) phase (Trenberth, 1984).

2.3. Multivariate ENSO Index Version 2 (MEIv2) Data

Multivariate ENSO index (MEI) is derived from five oceanic and atmospheric variables (Wolter & Timlin, 1998). It will also be used to explore the temporal and spatial variations of SIF, CO_2, and precipitation during El Niño months. Compared to SOI, the MEI includes information of more variables related to ENSO. In contrast to SOI, a positive (negative) MEI value indicates an El Niño (La Niña) phase (Wolter & Timlin, 1998).

2.4. NCEP2 Data

NCEP2 vertical pressure velocity at 500 hPa (Kanamitsu et al., 2002) is used in this study. In our previous studies (e.g., Jiang et al., 2023), we have found that the 500 hPa vertical pressure velocity is a good indicator for vertical transport in the mid-troposphere and exhibits a strong correlation with precipitation. The improved version (Reanalysis II) of the NCEP Reanalysis I model data is available through NOAA's Physical Sciences Laboratory (PSL). The improved Reanalysis II corrects errors and updates physical processes parametrizations (Kanamitsu et al., 2002). The spatial scale is 2.5° latitude × 2.5° longitude. The temporal scale covers monthly values from January 1979 to present.

2.5. GPCP Meteorological Data

We use Version 2.3 data from the GPCP for the precipitation analysis. The GPCP precipitation data is available through NOAA's PSL (Adler et al., 2018). The spatial scale is 2.5° latitude × 2.5° longitude. The temporal scale covers monthly values from January 1979 to present.

2.6. MODIS Burned Area Data and GFEDv4.1 CO_2 Surface Emissions Data

The MODIS burned area data, as described by Giglio et al. (2018), are utilized for estimating fire activities. To investigate CO_2 surface emissions during El Niño months, we rely on the GFEDv4.1 biomass burning emission and the CASA biosphere emission (Potter et al., 1993; Thompson et al., 1996).

2.7. CarbonTracker (CT2019B) Model

We will use NOAA's CarbonTracker (CT2019B) model to assess the accuracy of chemistry-transport models in predicting CO_2 variation over the Indo-Pacific region. The CarbonTracker simulates CO_2 measurements using global atmospheric CO_2 emissions (sources) and atmospheric CO_2 removals (sinks) (Jacobson et al., 2020).

Air-sea CO_2 exchange (Jacobson et al., 2007; Takahashi et al., 2009), CO_2 emissions from the biosphere (Potter et al., 1993), CO_2 emissions from biomass burning (Randerson et al., 2018), and fossil fuel emissions (Boden et al., 2017; Oda et al., 2018) are all considered in the CarbonTracker model.

3. Results

3.1. Temporal Variations of Different Variables

To study the temporal variation, we first compute the average of different variables over the entire Indo-Pacific region (10°S–10°N, 100°–160°E) to generate the regional-average time series. To focus on the interannual variations, we eliminate the annual cycles and semi-annual cycles of these variables from the time series. A filter is applied to the timeseries, and the signals corresponding to the 12-month and 6-month cycles are removed successfully from the timeseries. Figure S1a in Supporting Information S1 illustrates the CO_2 time-series after removing the annual and semi-annual cycles. The corresponding power spectrum is shown in Figure S1b in Supporting Information S1. As shown in Figure S1b in Supporting Information S1, the signals corresponding to the 12-month and 6-month cycles have been successfully removed from the CO_2 timeseries. The same analysis has been applied to all timeseries. A linear trend estimated through the least square fit is also eliminated from the time series of CO_2. The time series of averaged deseasonalized variables are displayed in Figure 1. Negative precipitation anomalies occur during the El Niño months (late 2015; Figure 1a) over the Indo-Pacific region, which is related to the change of the Walker Circulation. The warm pool will shift to the central Pacific in El Niño months (e.g., Bjerknes, 1966, 1969). Rising air will also shift from the western Pacific to the central Pacific, while sinking air are over the western Pacific. As shown in Figure 1a, there are positive 500 hPa vertical pressure velocities (sinking air) over the western Pacific during the El Niño months (late 2015), so there is less precipitation over the Indo-Pacific region during the El Niño. Less precipitation will lead to less photosynthesis from the vegetation; thus, the SIF values are low over the western Pacific during the El Niño months (late 2015; red line in Figure 1b). As a result, less photosynthetic activities will contribute to increased atmospheric CO_2 during the El Niño months (late 2015; black line in Figure 1c). For monthly CO_2 data averaged over 10°S–10°N, 100°–160°E (Figures 1c, 2c, and 3c), there are more than 35,000 OCO-2 retrievals for each data point. Since the standard error for each retrieval is 1.5 ppm, the CO_2 uncertainty for data in Figures 1c, 2c, and 3c is less than 0.1 ppm when we divide 1.5 ppm by the square root of number of retrievals (Jiang et al., 2023).

Figure 2a displays a scatter plot with a negative correlation between the precipitation and 500 hPa vertical pressure velocity from 2014 to 2019. The correlation coefficient between them is −0.95 (1% significance level; Jiang et al., 2004). To estimate a significance level, we first compute a normalized correlation distribution from the relevant indices and 3,000 isospectral time series, as described by Jiang et al. (2004). Then, we assess the actual correlation's significance in the normal distribution. A lower significance level indicates that the correlation coefficient is statistically significant (Jiang et al., 2004). Figure 2b displays a positive correlation between the precipitation and SIF from 2014 to 2019. The correlation coefficient between them is 0.79 (1% significance level). Figure 2c illustrates a plot between the SIF and CO_2, which suggests a weak anti-correlation, −0.20 (20% significance level), between them. Such a weak and insignificant correlation implies that atmospheric CO_2 is not determined only by photosynthetic activity (SIF), instead, atmospheric CO_2 is modulated by different variables, such as transport and CO_2 surface emission from fire (Albright et al., 2022; Jiang et al., 2023).

To further explore the impact of ENSO on precipitation, SIF, and CO_2, we conduct a comparative analysis between the ENSO indices (SOI and Inverted MEIv2) and these variables. Figure 3a illustrates positive correlations between deseasonalized precipitation and ENSO indices (SOI and Inverted MEI) with correlation coefficients of 0.65 (1% significance level) and 0.69 (1% significance level) for SOI and Inverted MEI, respectively. During El Niño months (September–December 2015), there is a decrease in precipitation due to sinking air over the Indo-Pacific region. This reduced precipitation during El Niño months will lead to a decline in photosynthetic activity. Deseasonalized SIF exhibits positive correlations with ENSO indices, showing correlation coefficients of 0.61 (1% significance level) and 0.69 (1% significance level) for SOI and inverted MEI, respectively. Negative SIF anomalies are observed in the Indo-Pacific region during El Niño months, which is associated with reduced photosynthetic activity and lower precipitation. During El Niño months (September–December 2015), there are positive CO_2 anomalies over the Indo-Pacific region due to diminished photosynthetic activities (low SIF) and increased biomass burning.
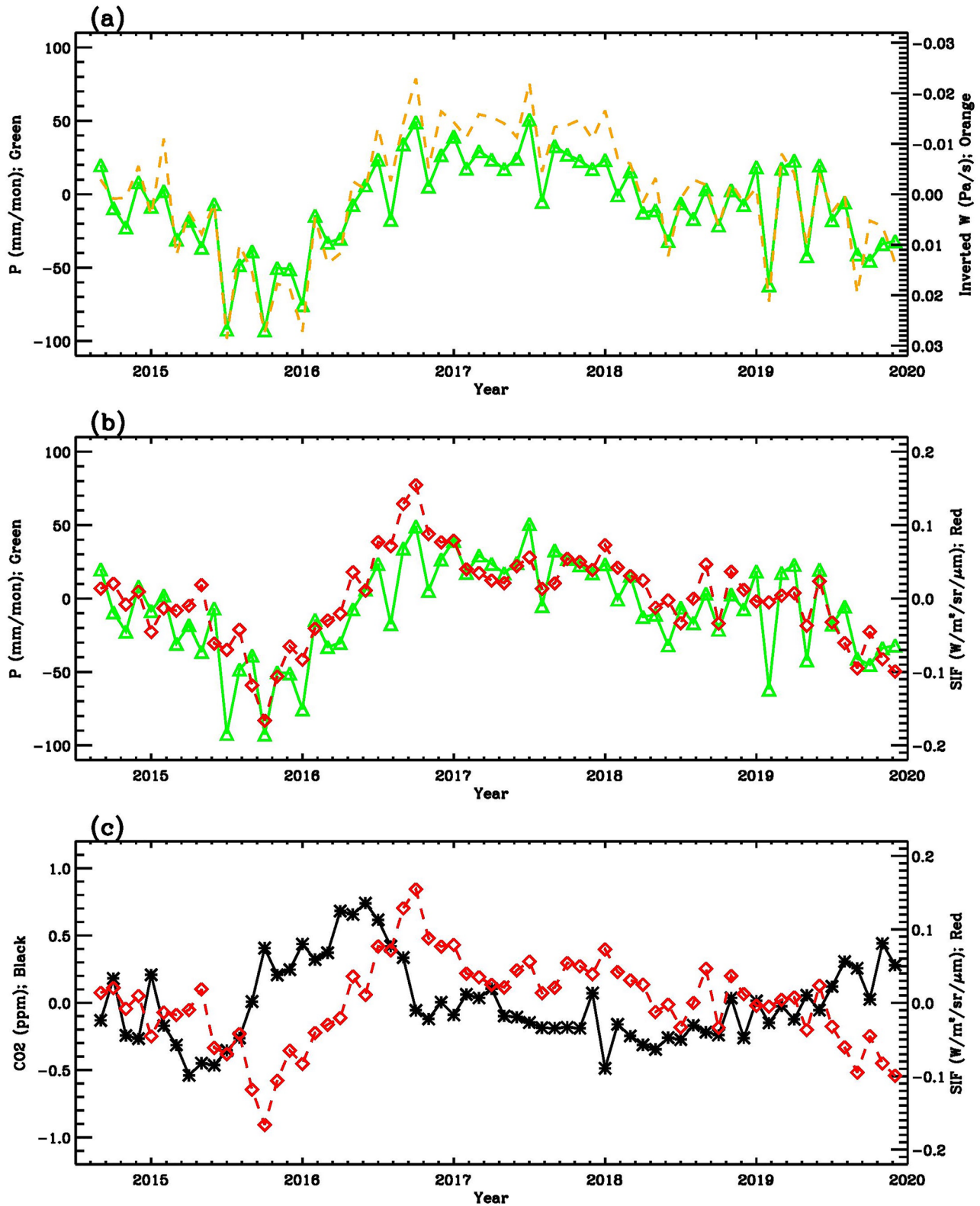
Figure 1. Panel (a) shows GPCP precipitation (green line) and 500 hPa inverted vertical pressure velocity (orange dashed line). Panel (b) shows GPCP precipitation (green line) and Orbiting Carbon Observatory 2 (OCO-2) Solar-Induced Fluorescence (SIF) (red dashed line). Panel (c) shows OCO-2 CO_2 (black line) and OCO-2 SIF (red dashed line). Data are averaged over 10°S–10°N, 100°–160°E.
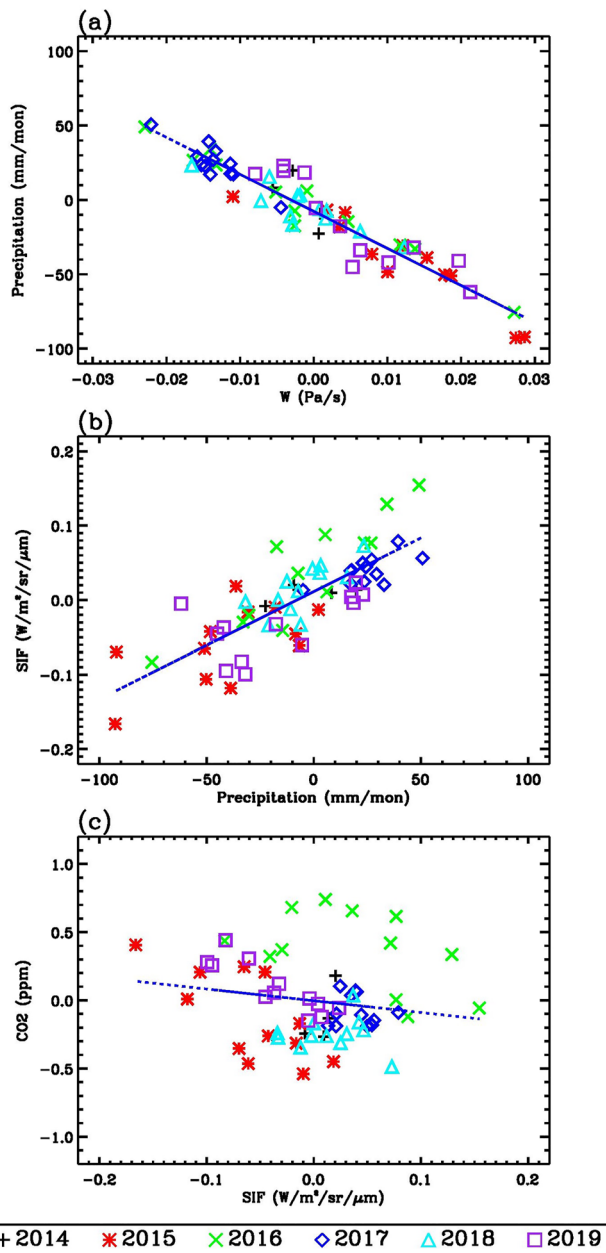
Figure 2. Panel (a) shows a scatter plot of the GPCP precipitation and vertical pressure velocity from 2014 to 2019. Panel (b) shows a scatter plot of the GPCP precipitation and Orbiting Carbon Observatory 2 (OCO-2) Solar-Induced Fluorescence (SIF) from 2014 to 2019. Panel (c) shows a scatter plot of the OCO-2 SIF and OCO-2 CO_2.

3.2. Spatial Variations of Different Variables

In Section 3.2, we investigate the spatial distributions of different variables across the Indo-Pacific region for the El Niño months and normal months. The average values of precipitation, burned area, SIF, and CO_2 during El Niño months (September–December 2015) and normal months (September–December 2016) are shown in Figures S2 and S3 in Supporting Information S1. We have chosen September–December 2015 as the El Niño months, for the MEI index is ~2 during these months, which is more than two standard deviations away from the mean MEI values and the ENSO signals are strongest during these time periods. Figure S2a in Supporting Information S1 shows that there is less precipitation (averaged precipitation is ~130 mm/month) over the Indo-Pacific region during El Niño months. This leads to more burned area (averaged value is ~0.95 × 10³ Ha), as indicated by Figure S2b in Supporting Information S1, and low SIF values (~0.7 W/m²/sr/μm), as indicated by Figure S2c in Supporting Information S1. Enhanced biomass burning and reduced photosynthetic activities result in higher atmospheric CO_2 concentrations over the Indo-Pacific region (Figure S2d in Supporting Information S1). Conversely, during the normal months (September–December 2016), there is more precipitation (~240 mm/month) over the Indo-Pacific region (Figure S3a in Supporting Information S1) due to rising air over the western Pacific region. Associated with more precipitation, there is less burned area (~0.2 × 10³ Ha; reduced fire activities; Figure S3b in Supporting Information S1) and high SIF values (~0.9 W/m²/sr/μm; enhanced photosynthetic activities; Figure S3c in Supporting Information S1). Reduced CO_2 biomass burning and strong photosynthetic activities result in lower atmospheric CO_2 over the Indo-Pacific region.

Differences of GPCP precipitation between (September–December 2015; El Niño months) and (September–December 2016; normal months) are shown in Figure 4a. There are negative precipitation anomalies over the Indo-Pacific region during the El Niño months. Differences in MODIS burned area between El Niño months and normal months are shown in Figure 4b. There is more burned area during the El Niño months than normal months. Associated with negative precipitation anomalies, there are negative SIF anomalies during the El Niño months (Figure 4c). Due to low SIF (photosynthesis) and high biomass burning, there are positive CO_2 anomalies over the Indo-Pacific region during the El Niño months than the normal months. The CO_2 difference between El Nino months and normal months can reach as high as 1.5 ppm, which is much greater than the uncertainty in CO_2 measurements (~0.1 ppm). For CO_2 data shown in Figure 4d, there are more than 700 OCO-2 retrievals for each grid cell. The CO_2 uncertainty for data in Figure 4d is less than 0.1 ppm when we divide 1.5 ppm by the square root of the number of retrievals. There are also negative CO_2 anomalies over the northeastern region of Papua New Guinea, which can be attributed to the negative net ecosystem exchange (NEE) of CO_2 as shown in Figure 5b.

3.3. Influence of ENSO on CO_2 Surface Emissions

The surface CO_2 emissions are important source of atmospheric CO_2. To enhance our understanding of the impact of ENSO on atmospheric CO_2, we analyzed averaged GFEDv4.1 CO_2 emissions data for El Niño months (September–December 2015) and normal months (September–December 2016), as presented in Figures S4 and S5 in Supporting Information S1. More CO_2 is released from the fire in the El Niño months (Figure S4a in Supporting Information S1), owing to reduced precipitation (dry weather) across the Indo-Pacific region. Additionally, Figure S4b in Supporting Information S1 demonstrates that CO_2 NEE is high over most regions of the
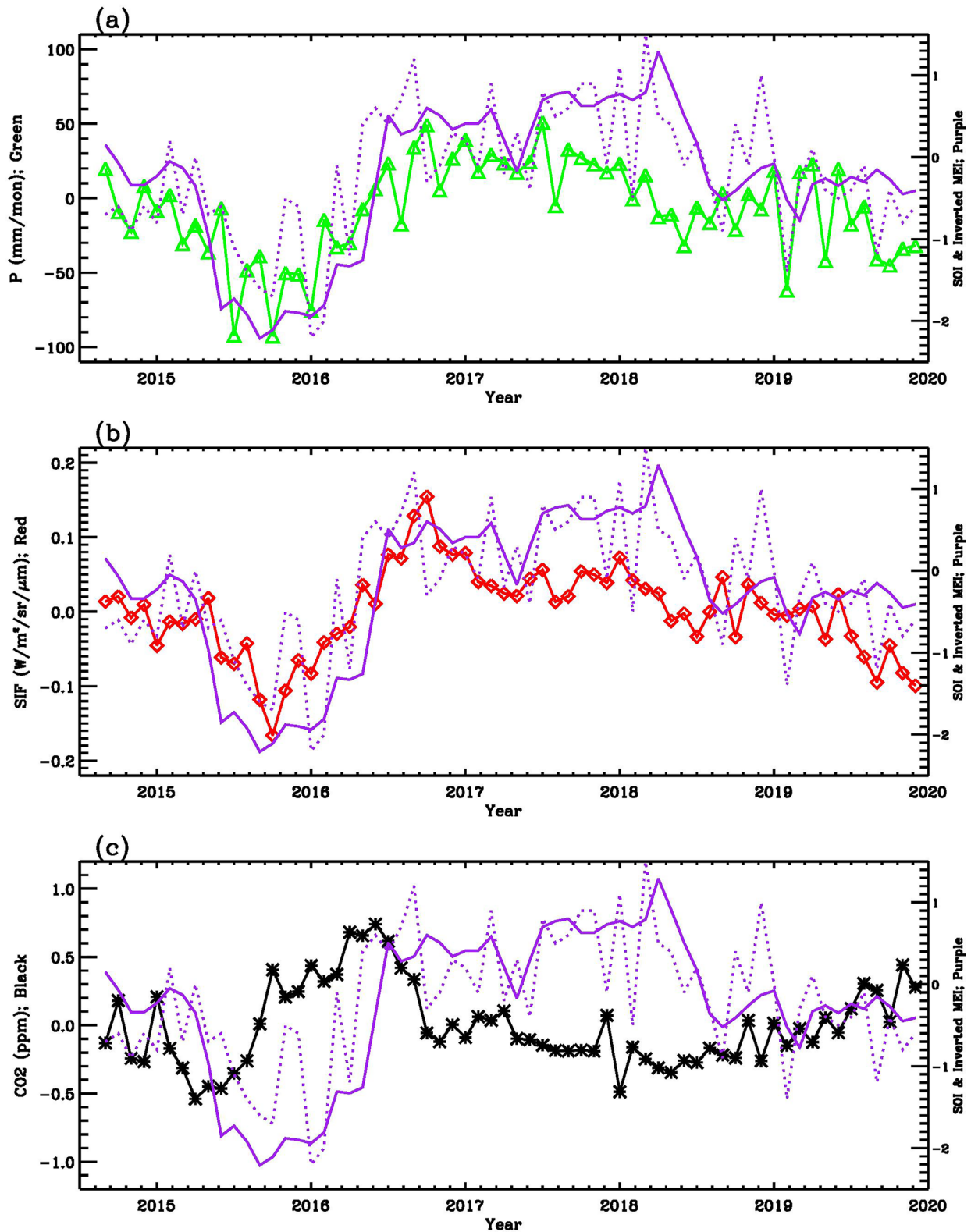
Figure 3. (a) Time series of GPCP precipitation (green line), Southern Oscillation Index (SOI) (purple dotted line), and inverted multivariate El Niño-Southern Oscillation index (MEI) (solid purple line). (b) Time series of Orbiting Carbon Observatory 2 (OCO-2) Solar-Induced Fluorescence (red line), SOI (purple dotted line), and inverted MEI (solid purple line). (c) Time series of OCO-2 CO_2 (black line), SOI (purple dotted line), and inverted MEI (solid purple line). Data are averaged over 10°S–10°N, 100°–160°E.
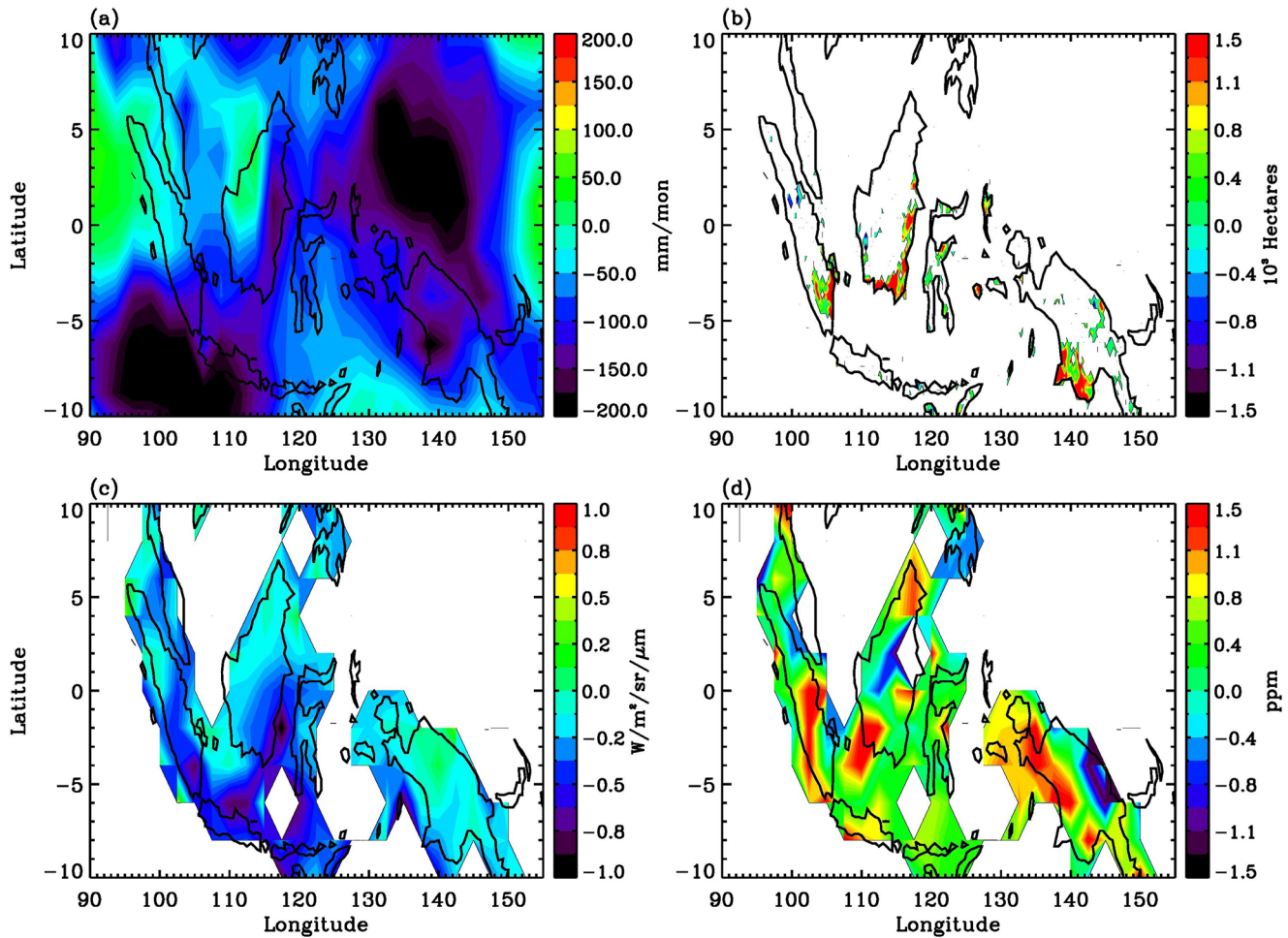
Figure 4. (a) Difference of GPCP precipitation between September–December 2015 and September-December 2016. (b) Difference of MODIS burned area between September–December 2015 and September–Decmber 2016. (c) Difference of Orbiting Carbon Observatory 2 (OCO-2) Solar-Induced Fluorescence between September–December 2015 and September–December 2016. (d) Difference of OCO-2 CO_2 between September–December 2015 and September–December 2016.

Indo-Pacific region during the El Niño months, leading to more CO_2 being emitted from the biosphere into the atmosphere, as a result of low photosynthetic activities across the same region (Figure S4d in Supporting Information S1). Figure S5 in Supporting Information S1 exhibits the results for the normal months (September–December 2016). During the normal months, CO_2 emissions from biomass burning are low due to high precipitation across the Indo-Pacific region. Moreover, CO_2 NEE is low during normal months (Figure S5b in Supporting Information S1) due to high photosynthetic activities (Figure S5d in Supporting Information S1). The differences in GFEDv4.1 CO_2 emissions between the El Niño months (September–December 2015) and the normal months (September–December 2016) are shown in Figure 5. As presented in Figure 5a, the El Niño months resulted in the release of more CO_2 from biomass burning than the normal months (September–December 2016). NEE shows positive (negative) anomalies over western (eastern) Indonesia, consistent with the anomalies in photosynthesis (Figure 5d). The photosynthesis patterns are similar to those obtained from the SIF results (Figure 4c).

3.4. CarbonTracker Model Analysis

To assess the performance of chemistry-transport models in simulating CO_2 variations over the Indo-Pacific region, we evaluate CO_2 simulations of NOAA's CarbonTracker model (Jacobson et al., 2020). Model CO_2 vertical profiles are convolved with the CO_2 averaging kernel from the OCO-2. Figure 6a shows the difference in CarbonTracker column CO_2 between September–December 2015 (El Niño months) and September–December 2016 (normal months). Higher model column CO_2 is seen over the Indo Pacific in the El Niño months than the normal months, which is similar to those from OCO-2 column CO_2. However, the model fails to capture the positive CO_2 anomalies
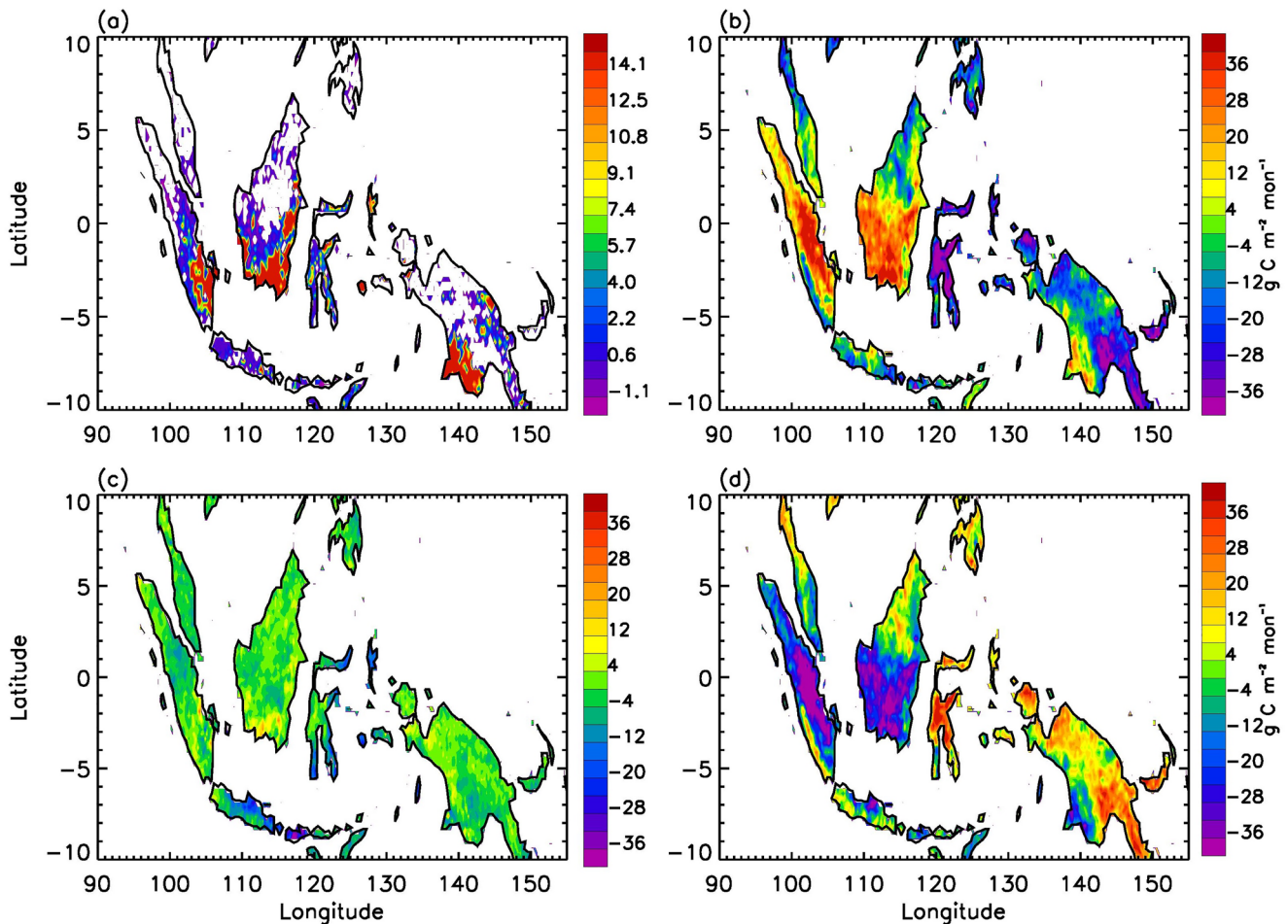
Figure 5. Difference of GFEDv4.1 data between September–December 2015 and September–December 2016. (a) CO_2 biomass burning emission, (b) CO_2 net ecosystem exchange, (c) CO_2 respiration, and (d) CO_2 photosynthesis.

over the eastern part of Indonesia. To better explore the difference between CarbonTracker model CO_2 and OCO-2 column CO_2, we estimate CarbonTracker CO_2 surface emission differences between El Niño months and normal months (Figure S6 in Supporting Information S1). As shown in Figure S6a in Supporting Information S1, more CO_2 is released from biomass burning during El Niño months (September–December 2015) than the normal months (September–December 2016), which is consistent with results from GFEDv4.1 biomass burning emissions (Figure 5a). The CarbonTracker CO_2 surface emissions from the biosphere (Figure S6b in Supporting Information S1) indicate positive anomalies in western Indonesia during El Niño months compared to normal months (Figure S6b in Supporting Information S1). However, it fails to capture the positive CO_2 biosphere emissions in Kalimantan Island and southern Papua Island, as depicted in the GFEDv4.1 NEE (Figure 5b). This might be a contributing factor to why the CarbonTracker model fails to capture the positive CO_2 anomalies in the eastern part of Indonesia.

Convolved model CO_2 is averaged over 10°S–10°N, 100°–160°E. Deseasonalized CarbonTracker column CO_2 (blue line) is compared to deseasonalized OCO-2 CO_2 (black line) in Figure 6b, with a correlation coefficient of 0.66 (1% significance level). The model can simulate temporal variations of CO_2 reasonably well. Model CO_2 is also compared to SOI (purple dotted line) and MEI (purple solid line). As shown in Figure 6b, CO_2 concentration increases during El Niño months over the Indo-Pacific region.

4. Conclusions

The selection of the Indo-Pacific region in this study was motivated by the presence of the third largest tropical rainforest (New Guinea Rainforest). Previous analyses (e.g., Jiang et al., 2021, 2023) have demonstrated that
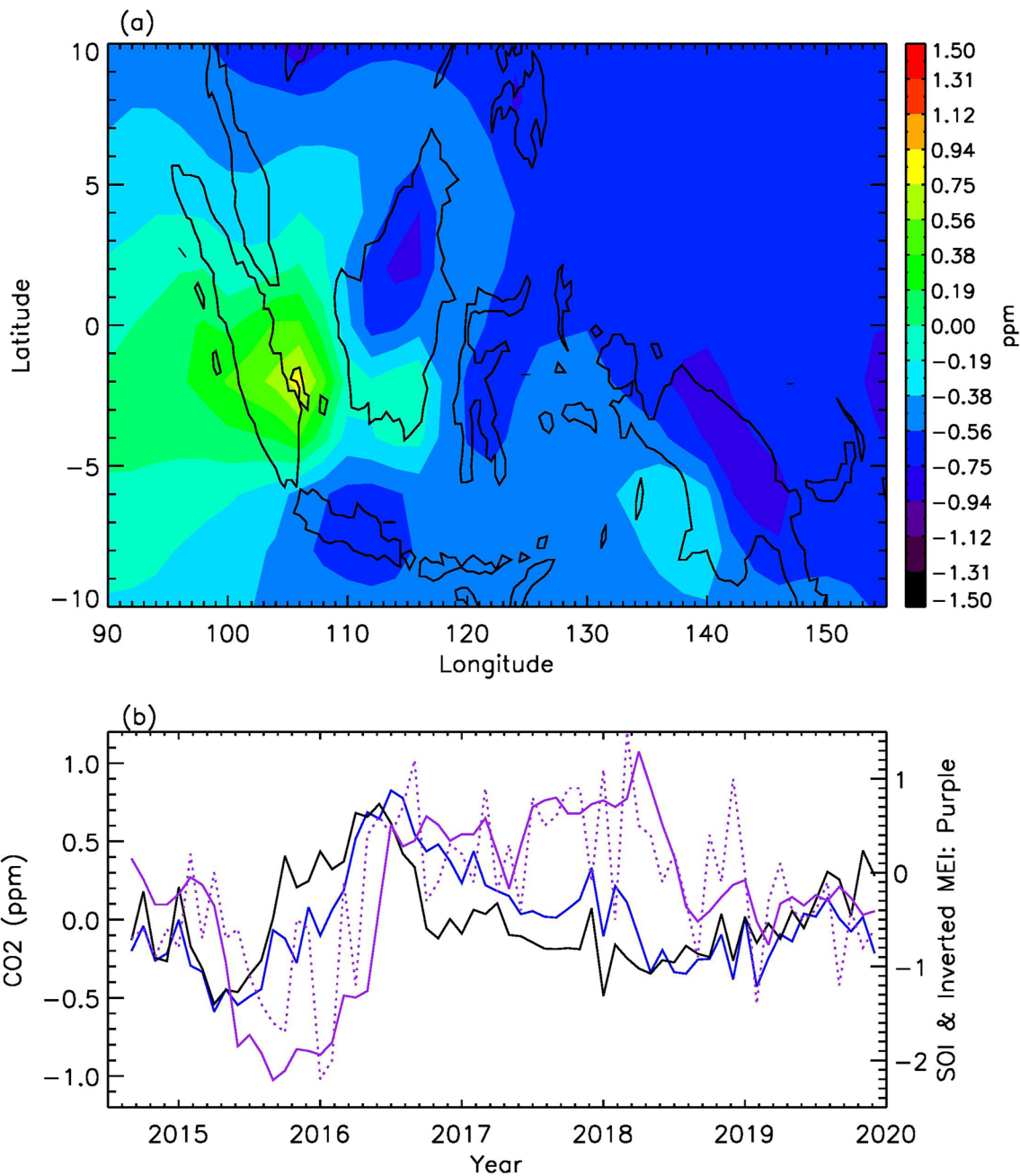
Figure 6. (a) Difference of CarbonTracker column CO_2 between September–December 2015 and September–December 2016. (b) Time series of CarbonTracker column CO_2 (blue line), Orbiting Carbon Observatory 2 CO_2 (black line), southern-oscillation index (SOI) (purple dotted line), and multivariate El Niño-Southern Oscillation index (solid purple line). Data are averaged over 10°S–10°N, 100°–160°E.

atmospheric CO_2 concentrations in the tropical rainforests (e.g., Amazon and Congo) are sensitive to variations in dry and wet conditions, which influence the photosynthetic activities of plants and the emissions from fires. During the dry/fire season, tropical rainforests transition from being carbon sinks to carbon sources (Jiang et al., 2023). The focus of our study is to examine the impacts of ENSO on the carbon budget within the third largest tropical rainforest, with a particular emphasis on investigating the variations of different variables (CO_2, precipitation, SIF, and burned area) across the Indo-Pacific region.

Our findings indicate that the Indo-Pacific region is directly influenced by ENSO events. Reduced precipitation during El Niño months (September–December 2015) over the Indo-Pacific region results in decreased

photosynthesis (indicated by reduced SIF) and increased biomass burning, leading to increased atmospheric CO_2 over the region. This suggests that the Indo-Pacific region (New Guinea Rainforest) shifts to a carbon source in the El Niño months, which is very important for the carbon budget over the rainforest region.

Given the significance of ENSO on forests, particularly in terms of CO_2 emissions from both biomass burning and photosynthesis, it is essential to get an accurate idea of how ENSO impacts CO_2 and SIF. Determining the impact of ENSO on CO_2 and SIF will help develop successful policies for climate change mitigation and adaptation efforts.

The comparative study between observational analyses and numerical simulations suggests that the current chemistry-transport models can capture the dominant influences of ENSO events on the regional-average CO_2 variations across the Indo-Pacific region. However, there are limitations in reproducing spatial pattern of CO_2 variations in some areas of the Indo-Pacific region (e.g., the eastern part of Indonesia). The observational characteristics from this study can help us develop these models by improving the simulations of ENSO's influence on CO_2, which further benefit the monitoring and prediction of this significant greenhouse gas.

Data Availability Statement

SIF data (Frankenberg et al., 2014) and CO_2 data (Crisp et al., 2017) from OCO-2 can be accessed at https://disc.gsfc.nasa.gov/datasets?keywords=oco-2&page=1. The NOAA SOI data (Trenberth, 1984) can be found at https://www.cpc.ncep.noaa.gov/data/indices/soi. For the GPCP precipitation data sets (Adler et al., 2018), you can find it at https://psl.noaa.gov/data/gridded/data.gpcp.html. MEIv2 data (Wolter & Timlin, 1998) are from https://psl.noaa.gov/enso/mei/. The MODIS burned area data (Giglio et al., 2018) are from http://modis-fire.umd.edu/. For GFEDv4.1 data (Randerson et al., 2018), you can find it at https://daac.ornl.gov/VEGETA-TION/guides/fire_emissions_v4_R1.html. CarbonTracker CT2019B model CO_2 (Jacobson et al., 2020) can be downloaded from https://gml.noaa.gov/ccgg/carbontracker/index.php. We list websites for all data in Table S1 in Supporting Information S1.

References

Adler, R. F., Sapiano, M. R. P., Huffman, G. J., Wang, J., Gu, G., Bolvin, D., et al. (2018). The global precipitation climatology project (GPCP) monthly analysis (new version 2.3) and a review of 2017 global precipitation [Dataset]. *Atmosphere*, *9*(4), 9. https://doi.org/10.3390/atmos9040138

Albright, R., Corbett, A., Jiang, X., Creecy, E., Newman, S., Li, K. F., et al. (2022). Seasonal variations of Solar-Induced Fluorescence, precipitation, and carbon dioxide over the Amazon. *Earth & Space Science*, *9*(1), e2021EA002078. https://doi.org/10.1029/2021EA002078

Bacastow, R. B. (1976). Modulation of atmospheric carbon dioxide by the Southern Oscillation. *Nature*, *261*(5556), 116–118. https://doi.org/10.1038/261116a0

Bjerknes, J. (1966). A possible response of the Atmospheric Hadley Circulation to equatorial anomalies of ocean temperature. *Tellus*, *18*(4), 820–829. https://doi.org/10.1111/j.2153-3490.1966.tb00303.x

Bjerknes, J. (1969). Atmospheric teleconnections from the equatorial Pacific. *Journal of Physical Oceanography*, *97*(3), 163–172. https://doi.org/10.1175/1520-0493(1969)097<0163:atftep>2.3.co;2

Boden, T. A., Marland, G., & Andres, R. J. (2017). *Global, regional, and national fossil fuel CO_2 emissions*. Carbon Dioxide Information Analysis Center, Oak Ridge National Laboratory, U.S. Department of Energy.

Crisp, D., Pollock, H. R., Rosenberg, R., Chapsky, L., Lee, R. A. M., Oyafuso, F. A., et al. (2017). The on-orbit performance of the Orbiting Carbon Observatory-2 (OCO-2) instrument and its radiometrically calibrated products [Dataset]. *Atmospheric Measurement Techniques*, *10*(1), 59–81. https://doi.org/10.5194/amt-10-59-2017

Feely, R., Gammon, R. H., Taft, B. A., Pullen, P. E., Waterman, L. S., Conway, T. J., et al. (1987). Distribution of chemical tracers in the eastern equatorial Pacific during and after the 1982-1983 El Niño/Southern Oscillation event. *Journal of Geophysical Research*, *92*(C6), 6545–6558. https://doi.org/10.1029/jc092ic06p06545

Feely, R., Takahashi, T., Wanninkhof, R., McPhaden, M. J., Cosca, C. E., Sutherland, S. C., & Carr, M. (2006). Decadal variability of the air-sea CO_2 fluxes in the equatorial Pacific Ocean. *Journal of Geophysical Research*, *111*(C8), C08S90. https://doi.org/10.1029/2005JC003129

Francey, R., Tans, P. P., Allison, C. E., Enting, I. G., White, J. W. C., & Trolier, M. (1995). Changes in oceanic and terrestrial carbon uptake since 1982. *Nature*, *373*(6512), 326–330. https://doi.org/10.1038/373326a0

Frankenberg, C., O'Dell, C., Berry, J., Guanter, L., Joiner, J., Kohler, P., et al. (2014). Prospects for chlorophyll fluorescence remote sensing from the Orbiting Carbon Observatory-2 [Dataset]. *Remote Sensing of Environment*, *147*, 1–12. https://doi.org/10.1016/j.rse.2014.02.007

Giglio, L., Boschetti, L., Roy, D., Hoffmann, A. A., Humber, M., & Hall, J. V. (2018). Collection 6 MODIS burned area product user's guide version 1.2 [Dataset]. Retrieved from http://modis-fire.umd.edu/files/MODIS_C6_BA_User_Guide_1.2.pdf

IPCC. (2013). In T. F. Stocker, D. Qin, G. K. Plattner, M. Tignor, S. K. Allen, J. Boschung, et al. (Eds.), *Climate change 2013: The physical science basis. Contribution of working group I to the fifth assessment report of the intergovernmental panel on climate change*. Cambridge University Press.

Jacobson, A. R., Gruber, N., Sarmiento, J. L., Gloor, M., & Fletcher, S. E. M. (2007). A joint atmosphere-ocean inversion for surface fluxes of carbon dioxide: I. Methods and global scale fluxes. *Global Biogeochemical Cycles*, *21*(1), GB1019. https://doi.org/10.1029/2005GB002556

Jacobson, A. R., Schuldt, K. N., Miller, J. B., Oda, T., Tans, P., Mund, J., et al. (2020). CarbonTracker CT 2019B [Dataset]. Global Monitoring Laboratory. https://doi.org/10.25925/20201008

Jiang, X., Albright, R., Creecy, E., Li, K., Liang, M., Newman, S., et al. (2023). Congo basin rainforest is a net carbon source during the dry season. *Earth & Space Sciences*, *10*(2), e2022EA002644. https://doi.org/10.1029/2022EA002644

Jiang, X., Camp, C. D., Shia, R., Noone, D., Walker, C., & Yung, Y. L. (2004). Quasi-biennial oscillation and quasi-biennial oscillation–annual beat in the tropical total column ozone: A two-dimensional model simulation. *Journal of Geophysical Research*, *109*(D16), D16305. https://doi.org/10.1029/2003JD004377

Jiang, X., Chahine, M. T., Olsen, E. T., Chen, L. L., & Yung, Y. L. (2010). Interannual variability of mid-tropospheric CO_2 from atmospheric infrared sounder. *Geophysical Research Letters*, *37*(13), L13801. https://doi.org/10.1029/2010GL042823

Jiang, X., Li, K. F., Liang, M. C., & Yung, Y. L. (2021). Impact of Amazonian fires on atmospheric CO_2. *Geophysical Research Letters*, *48*(5), e2020GL091875. https://doi.org/10.1029/2020GL091875

Jiang, X., & Yung, Y. L. (2019). Global patterns of carbon dioxide variability from satellite observations. *Annual Review of Earth and Planetary Sciences*, *47*(1), 225–245. https://doi.org/10.1146/annurev-earth-053018-060447

Jones, C. D., Collins, M., Cox, P. M., & Spall, S. A. (2001). The carbon cycle response to ENSO: A coupled climate-carbon cycle model study. *Journal of Climate*, *14*(21), 4113–4129. https://doi.org/10.1175/1520-0442(2001)014<4113:tccrte>2.0.co;2

Kanamitsu, M., Ebisuzaki, W., Woollen, J., Yang, S.-K., Hnilo, J. J., Fiorino, M., & Potter, G. L. (2002). NCEP-DOE AMIP-II Reanalysis (R-2). *Bulletin of the American Meteorological Society*, *83*(11), 1631–1643. https://doi.org/10.1175/BAMS-83-11-1631(2002)083<1631:NAR>2.3.CO;2

Keeling, C. D., Whorf, T. P., Wahlen, M., & Vanderplicht, J. (1995). Interannual extremes in the rate of rise of atmospheric carbon dioxide since 1980. *Nature*, *375*(6533), 666–670. https://doi.org/10.1038/375666a0

Lan, X., Tan, P., & Thoning, K. W. (2023). Trends in globally-averaged CO_2 determined from NOAA global monitoring laboratory measurements. Version 2023-05. Retrieved from https://www.esrl.noaa.gov/gmd/ccgg/trends/

Li, K. F., Tian, B., Waliser, D. E., & Yung, Y. L. (2010). Tropical mid-tropospheric CO_2 variability driven by the Madden-Julian Oscillation. *Proceedings of the National Academy of Sciences of the United States of America*, *107*(45), 19171–19175. https://doi.org/10.1073/pnas.1008222107

Liu, J., Bowman, K. W., Schimel, D. S., Parazoo, N. C., Jiang, Z., Lee, M., et al. (2017). Contrasting carbon cycle responses of the tropical continents to the 2015-2016 El Niño. *Science*, *358*(6360), eaam5690. https://doi.org/10.1126/science.aam5690

Oda, T., Maksyutov, S., & Andres, R. J. (2018). The open-source data inventory for anthropogenic CO_2 version 2016 (ODIAC2016): A global monthly fossil fuel CO_2 gridded emissions data product for tracer transport simulations and surface flux inversions. *Earth System Science Data*, *10*(1), 87–107. https://doi.org/10.5194/essd-10-87-2018

Potter, C. S., Randerson, J. T., Field, C. B., Matson, P. A., Vitousek, P. M., Mooney, H. A., & Klooster, S. A. (1993). Terrestrial ecosystem production: A process model based on global satellite and surface data. *Global Biogeochemical Cycles*, *7*(4), 811–841. https://doi.org/10.1029/93gb02725

Randerson, J. T., van der Werf, G. R., Giglio, L., Collatz, G. J., & Kasibhatla, P. S. (2018). Global fire emissions database, version 4.1 (GFEDv4) [Dataset]. ORNL DAAC. Retrieved from https://daac.ornl.gov/VEGETATION/guides/fire_emissions_v4_R1.html

Takahashi, T., Sutherland, S. C., Wanninkhof, R., Sweeney, C., Feely, R. A., Chipman, D. W., et al. (2009). Climatological mean and decadal change in surface ocean pCO_2, and net sea-air CO_2 flux over the global oceans. *Deep Sea Research Part II: Topical Studies in Oceanography*, *56*(8–10), 554–577. https://doi.org/10.1016/j.dsr2.2008.12.009

Thompson, M. V., Randerson, J. T., Malmstrom, C. M., & Field, C. B. (1996). Change in net primary production and heterotrophic respiration: How much is necessary to sustain the terrestrial carbon sink. *Global Biogeochemical Cycles*, *10*(4), 711–726. https://doi.org/10.1029/96gb01667

Trenberth, K. E. (1984). Signal versus noise in the southern oscillation [Dataset]. Monthly Weather Review, *112*(2), 326–332. https://doi.org/10.1175/1520-0493(1984)112<0326:SVNITS>2.0.CO;2

Wolter, K., & Timlin, M. S. (1998). Measuring the strength of ENSO events – How does 1997/98 rank? [Dataset]. Weather, *53*(9), 315–324. https://doi.org/10.1002/j.1477-8696.1998.tb06408.x

Wunch, D., Wennberg, P. O., Osterman, G., Fisher, B., Naylor, B., Roehl, C. M., et al. (2017). Comparisons of the orbiting carbon observatory-2 (OCO-2) XCO_2 measurements with TCCON. *Atmospheric Measurement Techniques*, *10*, 2209–2238. https://doi.org/10.5194/amt-10-2209-2017

Yu, L., Wen, J., Chang, C. Y., Frankenberg, C., & Sun, Y. (2018). High-resolution global contiguous SIF of OCO2. *Geophysical Research Letters*, *46*(3), 1449–1458. https://doi.org/10.1029/2018gl081109